RSC Advances

ROYAL SOCIETY OF CHEMISTRY

www.rsc.org/advances

Realizing simultaneous reinforcement and toughening in polypropylene based on polypropylene/elastomer via controlling crystalline structure and dispersed phase morphology

Jianfeng Wang, Hong Wu*, Shaoyun Guo*

The State Key Laboratory of Polymer Materials Engineering, Polymer Research Institute of Sichuan University, Chengdu 610065, China

Abstract

In this work, an advanced extrusion approach (MSEDC technique) was adopted to control crystalline structure and phase morphology in PP/POE blends. The results showed that PP matrix alternating shish-kebab crystalline structure with spherulites, and POE phase alternating micro-/nano-sheets with nano-fibrils and elongated spherical particles were introduced into PP/POE blends simultaneously. The as-obtained densely-stacked shish-kebab crystalline structure of PP matrix can provide blends with greatly enhanced tensile yield strength, while the planar POE phase with micro-/nano-sheets can induce the deflection of crack, providing the blends with greatly increased toughness. Moreover, hierarchical interfacial entanglement, formed between PP molecules and POE molecules, can connect the matrix and dispersed phase effectively, which is helpful to obtain materials with simultaneously enhanced strength and toughness. Compared with neat PP, the notched impact strength and tensile yield strength of MSEDC PP/POE blends enhanced 490% and 35%, respectively, which is the first report realizing simultaneous reinforcement and toughening in polypropylene based on polypropylene/elastomer binary system.

Keywords: Polypropylene; reinforcement and toughening; structure design; structure-properties relationship

Introduction

Over the past decades, polymer toughening has attracted considerable scientific

* To whom correspondence should be addresses. (Prof. Wu, Email: wh@scu.edu.cn, Fax: 86-028-85466077)
* To whom correspondence should be addresses. (Prof. Guo, Email: sguo@scu.edu.cn, Fax: 86-028-85405135)

and industrial interest because the application of many polymers is greatly restricted due to their poor toughness. Blending with elastomer is considered as a simple and feasible way to improve the toughness of polymer matrix. Unfortunately, because of the low modulus of the elastomer, the rigidity of the polymer/elastomer blends tends to decrease dramatically, especially when it needs to obtain materials with greatly enhanced toughness. Adding rigid filler [1-4] like carbon filler, nano-$CaCO_3$, clay, SiO_2, to prepare polymer/elastomer/rigid filler ternary system was proposed to be one effective method to overcome the rigidity loss in polymer blends resulting from the addition of elastomer. However, it has been found that the dispersed phase morphology and microstructure of ternary system are very difficult to control, which greatly restrict the mass fabrication of polymer composites with excellent and balanced mechanical properties. Therefore, searching for a potential and feasible strategy to obtain highly toughened polymer blends without rigidity sacrifice or even with enhanced rigidity is highly desirable.

In fact, even though many factors [5-7] have the influence on the final properties of polymer/elastomer binary system, dispersed phase morphology and super-molecular structure of matrix are considered two intrinsic factors in determining the properties of polymer/elastomer blends. It has been well documented that the toughening effect of the dispersed phase of planar elastomer like ellipsoid [8-10] or layered [11] was better than that of their conventional spherical counterparts. Unfortunately, the strength of matrix in these polymer blends [8-11] with planar elastomer phase morphology was not improved effectively due to the lack of consideration in designing the super-molecular structure of polymer matrix, like molecular conformation and crystalline structure. Moreover, it has been proved that the strength of the matrix could be enhanced via introducing some special super-molecular structures, like molecular orientation [12] and shish-kebab structure [13, 14], although the introduction of these super-molecular structure were not always beneficial to improve the toughness of the polymer matrix. So it can be found that the planar elastomer dispersed phase and shish-kebab crystalline of matrix are favorable to enhance the toughness and strength of polymer matrix, respectively. Unfortunately,

however, almost no literature has reported to introduce these two decisive and positive factors into polymer composites toughened with elastomer, to tailor the mechanical properties of polymer/elastomer blends.

On the other hand, it is well-known that polymer matrix with molecular orientation or shish-kebab crystalline structure was always induced through shearing force or extensional force [13-16]. Moreover, when it comes to the polymer/elastomer binary system during the melting process, dispersed phase morphology usually responded to the external stimulation (like shearing, extension) simultaneously with the super-molecular structure, which always leads to a complex hierarchical structure in the blends varying from microscopic super-molecular structure to macroscopic phase morphology [17, 18]. However, the dispersed phase morphology tended to form in-situ micro-fibrils [19-21] rather than planar micro-sheets under shearing force or extensional force, which has been proved to be adverse for toughening polymer matrix [18, 19]. Therefore, it is still a challenge to search for a potential approach to introduce planar dispersed phase as well as shish-kebab crystalline structure into the same toughening system.

In this paper, a novel extrusion technique, MSEDC approach (seen in Fig.1), was adopted to tailor the dispersed phase morphology and super-molecular structure of polypropylene/poly (ethylene-co-octene) blends (PP/POE), a typical elastomer-toughened thermoplastic system. The MSEDC approach includes two parts: multi-stretched extrusion [22, 23], and subsequent drawing and calendaring. As seen in Fig.1(c), the multi-stretched extrusion part has a force assembly element (FAE), which can impose continuous shearing force on the melt, making the polymer molecules orient (seen in Fig.1(d)) and the phase morphology deform (seen in Fig.1(e)) along the flowing direction. The subsequent drawing, as shown in Fig.1(b), can impose extensional force on the gradually cooled melt, making the polymer molecules orient and the phase morphology deform along the flowing direction. Moreover, the subsequent calendaring is considered to provide melt with extensional force along the planar direction, making the phase morphology deform along the planar direction. Through the combinational technique above, PP matrix alternating

shish-kebab crystalline structure with spherulites, and POE phase alternating micro-/nano-sheets with nano-fibrils and elongated spherical particles were introduced into PP/POE blend simultaneously. The as-formed densely-stacked shish-kebab crystalline structure of PP matrix and planar dispersed POE phase can greatly enhance the rigidity and toughness of blends, respectively. The structure-properties relationship in MSEDC toughened system was discussed via exploring the potential toughening and reinforcing mechanism.

2 Experimental

2.1 Materials

The PP was of grade K1001 with a MFI of 1.0 g/10 min at 230 ˚C, 2.16 kg, supplied by Yan-Shan Petrochemical Co. The POE was Engage 8200 manufactured by Dow Chemical, with a MFI of 5.0 g/10 min, at 190 ˚C, 2.16 kg. Their densities were 0.905×10^3 and 0.870×10^3 kg/m^3, respectively.

2.2 Sample preparation

The PP/POE blends with weight ratios 80/20 was extruded through a twin-screw extruder. The temperature of mixing section was 175-195-210-205˚C from the hopper to the die. The PP/POE blends sheets were prepared through MSEDC technique with 0 and 6 force assembly elements (FAEs). The thickness of the extrude die was 2000μm; the distance between the extrude die and drawing rollers was 90mm; the distance between the top roller and the bottom roller was 600 μm. The drawing rate of the draw roller was 500 rpm. The overall sheet thickness was about 660μm. The as-obtained blends prepared through MSEDC technique with 0 and 6 FAEs are coded as M-0 and M-6, respectively. For comparison, conventional PP/POE blends (weight ratio 80/20) and neat PP samples were prepared without multi-stretched extrusion and subsequent drawing and calendaring, and were coded as C-20 and C-0, respectively.

2.3 Mechanical properties test

The notched Izod impact strength was tested following GB/ 1943-2007 with a XJU-22 impact test machine. The fracture direction is parallel to the thickness direction. The sample, whose size was 80×10×4 mm^3, was prepared though a compression molding of the PP/POE sheets at 180 ˚C under the pressure of 10 MPa,

and then through post-treatment of cutting and polishing. The depth of the notch was 2.0 mm. Standard tensile test was conducted at room temperature using tensile test machine (model CMT-4104) according to GB/T 1040-92. The dumbbell shaped sample, prepared directly with the extruded sheets, was tested along the flowing direction at a tensile rate of 100 mm/min. Each impact test included five parallel experiments, and the results were averaged.

2.4 Polarized optical microscopy (POM)

Polarized optical microscopy (POM, BX51, Olympus) was used to observe the non-isothermal crystalline kinetics behavior of PP/POE blends. A 15-μm slice sample was cut from the extruded sheets along the melt flowing direction using a rotary microtome (YD-2508B). In order to observe the crystallization kinetics of PP/POE blends, the specimen was melt-pressed between two cover glasses on a hot stage (INSTEC HCS302) at 180˚C and equilibrated at for 5 min. The melted specimen was cooled down to 160˚C with a cooling rate 10˚C/min, and then cooled down to 100˚C with a cooling rate 2˚C/min. Structural development during the cooling scan was observed under the optical microscope equipped with a video recording system and exposure control unit.

On the other hand, the crack initiation and propagation stage were observed through a part-impact test, which was performed with the XJU-22 impact test machine. The pendulum was raised at an angle of 50° and 90° from the vertically fixed specimen, and then released to hit the specimen. The specimen was not broken into two halves as expected, and the propagating crack stopped in the interior of the specimen. The initiation and propagation patterns of crack were collected by POM, with the 30-μm sample slices cut from part-impact specimens along the crack propagation direction but perpendicular to the impact direction. The pictures collected by POM were all recorded with a Pixelink camera (PL-A662).

2.5 Scanning electron microscopy (SEM)

Scanning electron microscopy (SEM, JSM-5900LV, Japan) were performed to examine the impact-fractured surfaces, crystalline structure of the matrix and the dispersed phase morphology. The morphology of dispersed POE phase was obtained

by cryo-fracture the samples parallel to the flowing direction and planar direction quenched in liquid nitrogen and then etched in heptane at 75 ˚C for 6 h. Besides, the samples fractured parallel to the flowing direction were also etched in permanganate-acid solution [24] at room temperature for 50 h to observe the crystalline structure of the matrix. The surfaces were coated with gold before the SEM test.

2.6 FTIR and Polarized-FTIR test

The orientation function of PP molecules and POE molecules from the skin to the core along the thickness direction were monitored by a Thermo Nicolet infrared microscope. The IR source was provided by a Thermo Nicolet FTIR spectrometer with a resolution of 2 cm^{-1} and an accumulation of 32 scans. The test slice sample with thickness of 20 μm was cut by the rotary microtome (YD-2508B) along the flowing direction directly from the extruded sheets. Polarized infrared spectra, parallel and perpendicular to sampling region, respectively, were collected by rotating a ZnSe polarizer. Moreover, in order to qualitatively characterize the orientation direction of different regions in PP molecules and POE molecules, FTIR spectra were also recorded as a function of the angle of rotation in the transmittance mode when the polarizer was rotated.

The orientation function f, dichroic ratio R and structural absorbance A of a desired absorption band are deduced using the following equations [25]:

$$f = \frac{R-1}{R+2} \quad (1)$$

$$R = \frac{A_{\parallel}}{A_{\perp}} \quad (2)$$

Where $A_{\parallel}$ and $A_{\perp}$ are the parallel and perpendicular absorbance at the same positions, respectively. To determine the dichroic ratio (R) of polypropylene, as is well-known, bands at 998cm^{-1} are usually used to evaluate the PP crystalline phase (f_c) and bands at 973cm^{-1} are used to estimate both crystalline and amorphous phase (f_{av}) [25]. Besides, bands at 720cm^{-1} are used to evaluate the vibration of side hexyl chain on

POE molecules [26].

3 Results and discussion

3.1 Molecular orientation

It is well-known that the super-molecular structure of crystalline polymer is very sensitive to processing parameters such as thermal conditions and stress field [27]. Herein, micro-polarized FTIR [28] was performed to investigate the molecular orientation of conventional blends and MSEDC blends. Micro-polarized FTIR measurements were conducted on C-20 and M-6 as a function of the rotation angle of the specimen and the measured peak intensities of selected IR bands were plotted with respect to the rotation angle of the specimen, as a polar diagram. As shown in Fig.2, it is clear that absorbance intensity at 998cm^{-1} and 973cm^{-1} shows a maximum along the direction 0↔180°, which is parallel to the melt flowing direction, but absorbance intensity shows a minimum along the direction 90↔270°, which is perpendicular to the melt flowing direction. This phenomenon indicates that the PP molecular chain in both crystalline phase and amorphous phase tend to orient along the flowing direction during MSEDC processing. In contrast, absorbance intensity at 720 cm^{-1} shows a maximum along the direction 90↔270° and a minimum of absorbance intensity along the direction 0↔180°. It can be ascribed that the bending vibration of the $(CH_2)_5$ side chain is perpendicular to the main chain of POE molecules. Moreover, the extensional stress between POE main chain and side chain increased with the increase of the shearing force and radial pressure resulting from multi-stretched and calendaring, which made the hexyl side chain orient perpendicular to the melt flowing direction.

On the other hand, orientation function (f) of the PP crystalline phase, average orientation function of both crystalline phase and amorphous phase, and orientation function of the hexyl side chain on POE molecules were calculated from the micro-polarized FTIR results according to equations (1)-(2), and plotted as a function of the distance from the skin, as shown in Fig.3. For C-20, the molecular orientation of the PP matrix and POE phase appears to be an isotropic-distributed structure with low orientation function. However, the molecular orientation in MSEDC blends presents a unique hierarchical distribution. For M-0 prepared through subsequent

drawing and calendaring, the orientation function of the PP component increased compared with that in C-20, due to the extensional force resulting from the subsequent drawing. Moreover, the orientation function appeared to be a hierarchical structure along the thickness direction. The orientation function in the region from about 70 μm to 300 μm away from the skin is the highest, called intermediate layer. Then the orientation function in the region from about 300 μm to the center along the thickness direction as well as that in the region less 20 μm away from the skin are the second highest, called skin layer and core layer, respectively. Interestingly, the orientation function presents a minimum in the region from about 20 μm to 70 μm, called sub-skin layer. The observed distribution of orientation function can be attributed to the hierarchical distribution of stress field in different regions. The molecular orientation in the skin layer is mainly attributed to the shearing stress induced by subsequent drawing, while the molecular orientation in the intermediate layer and the core layer is mainly ascribed to the synergistic effect of shearing force, extensional stress and radial pressure. Furthermore, the low thermal conductivity of polymers implies the thermal gradient along the thickness, indicating that the cooling rate and the relaxation time of molecular chain decrease from the skin toward the core. Therefore, the molecular orientation function in the core layer is lower than that in the intermediate layer. Besides, because of the radial pressure stress resulting from the drawing rollers, melt returning phenomenon may appear in the sub-skin layer, leading to the formation of "stress hollow" in this region. Therefore, the molecular orientation shows a minimum in the sub-skin layer.

For M-6 blends, the molecular orientation of PP molecules enhanced greatly compared with those in M-0, which was due to the great shearing force and extensional stress provided by the series of FAEs. The high molecular orientation function of the PP matrix in the MSEDC blends strongly implies the change on the crystalline structure. To speak of, the orientation distribution of the hexyl side chain on POE molecules is similar with that of PP molecules, expect for the orientation direction. The as-formed hierarchical distribution of orientation is also considered to have a great influence on the crystallization behavior, which will be discussed in

detail later.

3.2 Crystallization behavior analysis

Optical non-isothermal cooling images were performed, as seen in Fig.4, to explore the crystallization kinetics behavior of MSEDC blends and conventional blends. During the cooling process, randomly distributed nucleus appeared at 132 ˚C in C-20 (seen in Fig.4 (a)), and grew into big spherulites as the temperature decreased gradually. However, for MSEDC blends, during the identical cooling process (seen in Fig.4(b) and Fig.4(c)), orderly distributed row nucleus occurred at a higher temperature compared to that of C-20. For example, in M-6, a large area of long-range ordered row nucleus along the melt flowing direction appeared in the intermediate layer at 139 ˚C, a much higher temperature than that of C-20 (132 ˚C). And as the temperature decreased gradually, the area of the long-range ordered structure enlarged. At the same time, a small amount of disordered nucleus grew out in the core layer and sub-skin layer, and grew into spherulites gradually. This may be because long-range ordered crystal structure formed in the intermediate layer under the huge effect of multi-stress field. Moreover, a lot of ordered crystalline structure existed after being melted at 180 ˚C due to their relatively high melt temperature. Because of the memory effect of melt during the cooling process, the incompletely melted ordered crystals grew out preferentially and played the role of heterogeneous nucleation. When the temperature decreased continually, the PP lamellaes showed a strong epitaxial growth on the incompletely melted ordered crystals. Meanwhile, the crystal in the core layer and sub-skin layer started to grow in the form of homogeneous nucleation and finally grew into big spherulites. Moreover, the size of the spherulites in MSEDC blends decreased greatly compared with that in conventional blends.

To examine the effect of multi-stress filed during MSEDC process on the crystalline structure deeply, the sample of C-20 and M-6 was chemically etched by permanganate acid solution to remove the amorphous phase of the PP matrix (as well as POE). As shown in Fig.5, the crystalline structure of the PP matrix in M-6 also presented a hierarchical structure, which was very different from the well-developed spherulites in C-20. Typical shish-kebab structure with highly oriented and densely

stacked folded-chain lamellae, was formed in the intermediate layer and the skin layer in M-6. The folded-chain lamellae in the intermediate layer stacked more closely than that in the skin layer. Then well-developed spherulites were observed in the core layer and the sub-skin layer in M-6 (seen in Fig.5(b)), which were smaller than those in C-20 due to the confinement effect resulting from intermediate layer and skin layer. Moreover, a shish-kebab crystalline structure with large scale was detected in the boundary of the core layer and intermediate layer, which is considered to play the role of an effective connection between the two different crystalline structures: the spherulites in the core layer and the densely stacked shish-kebab structure in the intermediate layer.

3.3 Phase morphology and hierarchical structure

It is well-known that the morphology of elastomer like domain size and shape [29, 30] plays a vital role in determining the final properties of polymer/elastomer blends. Fig.6 and Fig.7 show the morphology of dispersed POE phase in M-0 and M-6, respectively. Unlike uniformly dispersed spherical POE phase in C-20 (seen Fig.S1 in support information), the dispersed POE phase in M-0 became irregular (seen in Fig.6). This can be attributed mainly to the effect of subsequent drawing and calendaring, which can impose extensional stress and radial pressure on the gradually cooled melt. Moreover, the stress field that POE particle subjected in different regions along the thickness direction was different. The external stress that POE phase subjected in the core layer was mainly shearing force and extensional force along the melt flowing direction. However, apart from the shearing force and extensional force along the melt flowing direction, POE phase in the intermediate layer was also subjected to radial pressure vertical to the melt flowing direction. Therefore, fiber-like and sheet-like phase morphology of POE particle appeared in the core layer and in the intermediate layer of M-0, respectively. This phenomenon also indicated that the spherical POE particle tended to evolve into sheet due to the existence of subsequent calendaring. Furthermore, for M-6, the dispersed POE phase formed in-situ short nano-fibrils in the core layer with averaged three-dimensional size 439×50×50 nm^3, and formed in-situ long nano-sheets in the intermediate layer with averaged

three-dimensional size 4190×1130×110 nm^3. The dispersed POE phase formed in-situ elongated particles in the skin layer and sub-skin layer. The formation of the hierarchical dispersed phase morphology may be ascribed to the different stress fields during the whole process. Under the effect of great shearing force in FAEs, the POE particle formed in situ micro-fibrils. And then extensional stress and radial pressure provided by subsequent drawing and calendaring made the micro-fibrils deform into nano-fibrils and micro-/nano-sheets. Therefore, a special hierarchical phase morphology alternating micro-/nano-sheets with nano-fibrils and elongated spherical particles was formed in MSEDC blends.

Combined with the above results, it is clear that a unique hierarchical structure along the thickness direction was introduced into PP/POE blends. A sketch of this hierarchical structure is shown in Fig.8. PP matrix alternating shish-kebab crystalline structure with spherulites and POE phase alternating micro-/nano-sheets with nano-fibrils and elongated spherical particles were introduced into PP/POE blends successfully. On the other hand, the interaction between PP molecules and POE molecules are also considered to be very different between conventional blends and MSEDC blends. As shown in Fig.8(a), most of the interfacial inter-entanglement in C-20 (form Ⅰ) takes place between the random molecular chains of PP molecules and POE molecules. However, apart from the inter-entanglement (form Ⅰ) similar with that in C-20, there are other two inter-entanglement forms in M-6. As shown in Fig.8(b), the first (form Ⅱ) takes place between oriented POE molecules and low-oriented PP molecules in the core layer, in which the entanglement point between PP molecules and POE molecules appear on the POE main molecules. The second (form Ⅲ) appears between oriented POE molecules and highly oriented PP molecules in the intermediate layer, in which most of the interfacial inter-entanglement take place in the inter-lamellar amorphous region. Moreover, the hexyl side chain on POE molecules, just like “hand” in the both sides of folded-chain lamellae, can also take part in the entanglement with PP molecules and enhance the interfacial interaction between the PP matrix and dispersed POE phase. The special interfacial entanglement between PP molecules and POE molecules can connect effectively the

super-molecular structure of matrix and dispersed POE phase morphology.

3.4 Mechanical properties

Fig.9 shows the typical strain-stress curves for C-0, C-20, M-0 and M-6 and table S1 (seen in support information) shows the mechanical properties of the above materials. It is clear that the addition of POE can effectively enhance the notched impact strength of the PP matrix (C-0), but the tensile yield strength of C-20 decreases dramatically compared with that of C-0. However, the tensile yield strength and impact strength of MSEDC blends are improved dramatically at the same time. Compared with the mechanical properties of C-0, the notched impact strength and tensile yield strength of M-6 enhance 490% and 35%, respectively. Meanwhile, compared with mechanical properties of C-20, the impact strength and tensile yield strength of M-6 increase 5% and 93%, respectively. Table 1 compares the mechanical increase ratio of PP composites toughened with different fillers. For most of the toughened composites, the strength of the matrix decreased to different extent, even though the toughness of matrix increased greatly. Few study, except for this work and the PP composites toughened with functional graphene oxide [24], realized the reinforcement and toughening PP matrix at the same time. According to Wu's theory [31], the spherical POE phase in C-20 can efficiency toughen PP matrix mainly due to the smaller ligament thickness. However, the situation for the MSEDC blends with unique hierarchical structure has hardly been reported before, so the potential toughening mechanism as well as the reinforcing mechanism in M-6 will be explored.

3.5 Fracture behavior and crack propagation

To ascertain the difference in the toughening mechanism between conventional blends and MSEDC blends, the impacted-fracture surface of C-20 and M-6 was studied, as shown in Fig.10. Although the fracture surface of C-20 and M-6 both presents a typical ductile fracture, the propagation patterns of the crack are very different. For conventional blends, the crack propagated mainly along the impact direction, especially in the region far away from the notch (Region B and C). However, for MSEDC blends, the crack not only propagated along the impact direction but also deflected at an angle from the impact direction (especially in the

region B and region C). In addition, some big cavities, which were absent on the fracture surface of C-20, occurred on the fracture surface of M-6.

On the other hand, the initiation and propagation patterns of the crack produced with the part-impact test were studied. Unlike classical observation on the crack propagation front, we observed the crack propagation pattern under two different stages: before and after the formation of the crack, as shown in Fig.11 and Fig.12, respectively. When the external impact force is insufficient to form crack, the color of the stress field is darker and the stress during the impact process in C-20 (dark zone) is more concentrated than that in M-6, which is much more favorable to the further formation of crack. It means that the crazing area in the MSEDC blends is larger than that in C-20 and the crack propagated as a larger angel from the cutting-edge of the crack than that in C-20 (seen in Fig.11). When the external impact force is sufficient to form cracks, as shown in Fig.12, the crack formed in M-6 is smaller than that in C-20. The area of stress concentration formed around the crack in M-6 is larger than that in C-20, and the color of stress field in M-6 became darker than that in C-20, which is different from that before the formation of crack. Moreover, the crack in C-20 tended to propagate as a fan-shaped zone, while the crack in M-6 tended to form a rectangle zone, which indicated the formation of crack deflection caused by the POE micro-/nano-sheets. The as-observed initiation and propagation patterns of the crack illustrate the advantage of the hierarchical structure in MSEDC blends on preventing the propagation of crack and improving the toughness over conventional blends.

3.6 Toughening and reinforcement mechanism

It is well-documented that the dispersed POE phase can initiate crazes and shear bands in blends as stress concentration factors [36], and then absorb the impact energy to block the crack propagation. In this work, during the impact process, the planar POE micro-/nano-sheets and elongated spherical particles can induce crack deflection perpendicular to the impact direction, transmit stress into PP matrix and make the PP matrix participate in the stress transmit more actively [11, 18]. This can absorb the impact energy along the impact direction and prevent the further development of craze into crack along the impact direction (seen in Fig.13(b)). This special

toughening mechanism is very different form that in conventional PP/POE blends with short-range ordered spherical POE phase, where the plastic deformation of the matrix could happen and the material could be successfully toughened only when the stress field around the rubbers overlap and pervade the matrix (seen in Fig.13(a)). So it could be well understood that the as-formed including micro-/nano-sheets and ellipsoid ones are beneficial to enhance the toughness of matrix.

Moreover, the crystalline structure of PP matrix is also of great importance on determining the toughness of blends. The spherulites in M-6 are smaller than those in C-20, which can increase the impact toughness of matrix. Moreover, compared with the densely stacked PP shish-kebab crystalline structure, the PP spherulites is more helpful to resist the external impact force, especially when the impact force is perpendicular to the oriented direction. So the existence of spherulites in the hierarchical crystalline structure could reduce the side-effect of molecular and crystalline orientation on toughening the matrix. Therefore, the as-formed hierarchical crystalline structure of PP matrix alternating shish-kebab crystalline structure with spherulites is beneficial from the toughening point of view.

On the other hand, the tensile deformation in semi-crystalline polymers was mainly attributed to the inter-lamellar and intra-lamellar slipping of the superstructure, chain pulling-out from the folded-chain lamellae, and re-crystallization and formation of oriented extended-chain crystals [37]. Moreover, the molecular orientation of the matrix is decisive factor on determining the tensile properties of oriented blends [38]. In the present work, the shish-kebab crystalline structure of PP matrix stacked densely and the molecules of the PP matrix oriented highly along the melt flowing direction. The intra-/inter- molecular interaction between PP molecules enhanced greatly in the as-formed special super-molecular structure, making the slipping of inter-/intra-molecule during tensile deformation more difficult and thus enhancing the tensile strength greatly. Therefore, the reinforcement of PP matrix in MSEDC blends is mainly attributed to the densely stacked shish-kebab crystalline structure with highly oriented molecules.

Of course, the dispersed POE phase in the PP matrix may make the stacked PP

molecules or folded-chain lamellae become loose, which will decrease the rigidity of PP matrix. So it can imagine that neat PP material with excellent rigidity can be obtained through the MSEDC approach.

4 Conclusions

Herein, we present a facile and efficient approach, MSEDC technique, to fabricate PP composites with balanced and excellent mechanical properties, which is based on elastomer-toughened PP binary system. Hierarchical structure of PP matrix alternating shish-kebab crystalline structure with spherulites and POE phase alternating micro-/nano-sheets with nano-fibrils and spheroidal particles were formed into PP/POE blends simultaneously. The formation of densely-stacked shish-kebab crystalline structure of PP matrix with highly oriented molecules was considered an important positive factor to increase the strength of matrix, while the as-obtained dispersed POE phase with planar micro-/nano-sheets can enhance the toughness of matrix dramatically. This work will not only give us insight into understanding the structure-property relationship but also shed some light on easy, feasible and scale fabrication of polymer-based materials with balanced and excellent mechanical properties and other functional materials require special hierarchical structure.

Acknowledgements

Financial support of the National Natural Science Foundation of China (51273132, 51227802 and 51421061), Program for New Century Excellent Talents in University (NCET-13-0392) and the Sichuan Province Youth Science Fund (2015JQ0015) are gratefully acknowledged.

References

[1] P. Dey, K. Naskar, B. Dash, S. Nair, G. Unnikrishnan and G.B. Nando, RSC. Adv., 2015, 5, 31886-31900.

[2] S. Bagheri-Kazemabad, D. Fox, Y.H. Chen, L.M. Geever, H.Z. Zhang and B.Q. Chen, Mater. Des., 2014, 53, 741-748.

[3] C.G. Ma, Y.L. Mai, M.Z. Rong, W.H. Ruan and M.Q. Zhang, Compos. Sci. Technol., 2007, 67, 2997-3005.

[4] H. Yang, Q. Zhang, M. Guo, C. Wang, R.N. Du and Q. Fu, Polymer, 2006, 47(6),

2106-2115

[5] H.W. Bai, D.Y. Bai, H. Xiu, H. Deng, F. Chen, Q. Fu and F.C. Chiu, RSC. Adv., 2014, 4, 49374-49385.

[6] Z. Zhang, X.J. Zhao, S.H. Wang, J. Zhang and W. Zhang, RSC. Adv., 2014, 4, 60617-60625.

[7] X.F. Wang, Z.X. Zhang, J.L. Li, J.H. Yang, Y. Wan and J.H. Zhang, RSC. Adv., 2015, 5, 69522-69533.

[8] J.F. Wang, C.L. Wang, X.L. Zhang, H. Wu and S.Y. Guo, RSC. Adv., 2014, 39, 20297-20307.

[9] S.L. Bai, G.T. Wang, J.M. Hiver and C. G'Sell, Polymer, 2004, 45, 3063-3071.

[10] C. Wang, J.X. Su, J. Li, H. Yang, Q. Zhang, R.N. Du and Q. Fu, Polymer, 2006, 47, 3197-3206.

[11] C.H. Li, S. Yang, J.F. Wang, H. Wu and S.Y. Guo, RSC. Adv., 2014, 4, 55119-55132.

[12] A. Kmetty, T. Barany and J.K. Kocsi, Prog. Polym. Sci., 2010, 35, 1288-1310.

[13] L. Zheng, Y.B. Quan, G.Q. Zheng, K. Dai, C.T. Liu and C.Y. Shen, RSC. Adv., 2015, 5, 60392-60400.

[14] Y.H. Huang, J.Z. Xu, J.S. Li, B.X. He, L. Xu and Z.M. Li, Biomaterials, 2014, 35(25), 6687-6697.

[15] H.W. Bai, C.M. Huang, H. Xiu, Q. Zhang, F. Chen and Q. Fu, Biomacromolecules, 2014, 15 (4), 1507–1514.

[16] R.H. Somani, L. Yang and B.S. Hsiao, Macromolecules, 2005, 38 (4), 1244–1255.

[17] K. Meng, X. Dong, X.H. Zhang, C.G. Zhang and C.C. Han, Macro. Rapid. Comm., 2006, 27, 1677-1683.

[18] H.N. Du, Y. Zhang, H. Liu, K. Liu, X.P. Li and J. Zhang, Polymer, 2014, 55, 5001-5012.

[19] C.Z. Geng, J.J. Su, S.J. Han, K. Wang and Q. Fu, Polymer, 2013, 54, 3392-3401.

[20] X.J. Sun, Q. Yu, J.B. Shen, S. Gao, J. Li and S.Y. Guo, J. Mater. Sci., 2013, 48, 1214-1224.

[21] J.F. Wang, X.L. Zhang, T.B. Zhao, L.Y. Shen, H. Wu and S.Y. Guo, J. Appl. Polym. Sci., 2014, 131, 40108-40116.

[22] G.S. He, J. Li, F.S. Zhang, C. Wang and S.Y. Guo, Compos. Sci. Technol., 2014, 100, 1-9.

[23] M. Wen, X.J. Sun, L. Su, J.B. Shen, J. Li and S.Y. Guo, Polymer, 2012, 53, 1602-1610.

[24] R.Y. Bao, J. Cao, Z.Y. Liu, W. Yang, B.H. Xie and M.B. Yang, J. Mater. Chem. A., 2014, 2, 3190-3199.

[25] S.H. Tabatabaei, P.J. Carreau and A. Ajji, J. Membr. Sci., 2008, 325, 772-782.

[26] J.F. Wang, J.W. Guo, C.H. Li, H. Wu and S.Y. Guo, J. Polym. Res., 2014, 21, 618-630.

[27] M. Fujiyama, T. Wakino and Y. Kavasaki, J. Appl. Polym. Sci., 1988, 35, 29-37.

[28] X. Wang, P. Zhang, Y. Chen, L.B. Luo, Y.W. Pang and X.Y. Liu, Macromolecules, 2011, 44, 9731-9737.

[29] X.L. Zhan, R. He, Q.H. Zhang and F.Q. Chen, RSC. Adv., 2014, 4, 51201-51207.

[30] F. Chen, B.W. Qiu, B. Wang, Y.G. Shangguan and Q. Zheng, RSC. Adv., 2015, 5, 20831-20837.

[31] S.H. Wu. Polymer, 1985, 26, 1855-1863.

[32] Y. Lin, H.B. Chen, C.M. Chan and J.S .Wu. Macromolecules, 2008, 41, 9204-9213.

[33] Z.S. Zhang, C.G. Wang, Y.Z. Meng and K.C. Mai, Compos. Part. A., 2012, 43(1), 189-197.

[34] R.B. Li, X.Q. Zhang, Y. Zhao, X.T. Hu, X.T. Zhao and D.J. Wang, Polymer, 2009, 50(21), 5124-5133.

[35] J.Z. Zheng, X.P. Zhou, X.L. Xie and Y.W. Mai, Nanoscale, 2010, 2: 2269-2274.

[36] G.Y. Liu and G.X. Qiu, Polym. Bull., 2013, 70, 849-857.

[37] R. Hiss, S. Hobeika, C. Lynn and G. Strobl, Macromolecules, 1999, 32, 4390-4403.

[38] B. Na, K. Wang, Q. Zhang, R.N. Du and Q. Fu, Polymer, 2005, 46, 3190-3198.

Table 1 Comparison of mechanical increase ratio of polypropylene composites toughened with different fillers.

Filler	Filler content (wt%)	Process Method	Maximum toughness enhancement (%)	Strength enhancement (%)	Reference
POE/nano-$CaCO_3$	5/7.5	Injection	452	–5	[3]
EPDM/SiO_2	20/5	Injection	1250	–34	[4]
POE	18	Multilayered co-extrusion	150	–15	[8]
PA/POE-g-MA	40/20	Injection molding	470	–9	[9]
POE	17	Multilayered co-extrusion	193	–25	[11]
POE/ β-nucleating agent	10/0.05	Injection molding	1476	–21	[18]
GO-β-nucleating agent	0.1	Solution	100	30	[24]
SEP	15	Compression molding	216	–15	[30]
nano-$CaCO_3$	20	Injection molding	342	–8	[32]
nano-$CaCO_3$/β-nucleating agent	5/0.1	Injection molding	141	-5	[33]
EP-P	40	Extrusion	2600	–32	[34]
Si/poly(MMA-co-BA)	5/2.5	Injection	105	–3	[35]
POE	***20***	***MSEDC***	***490***	***35***	***this work***

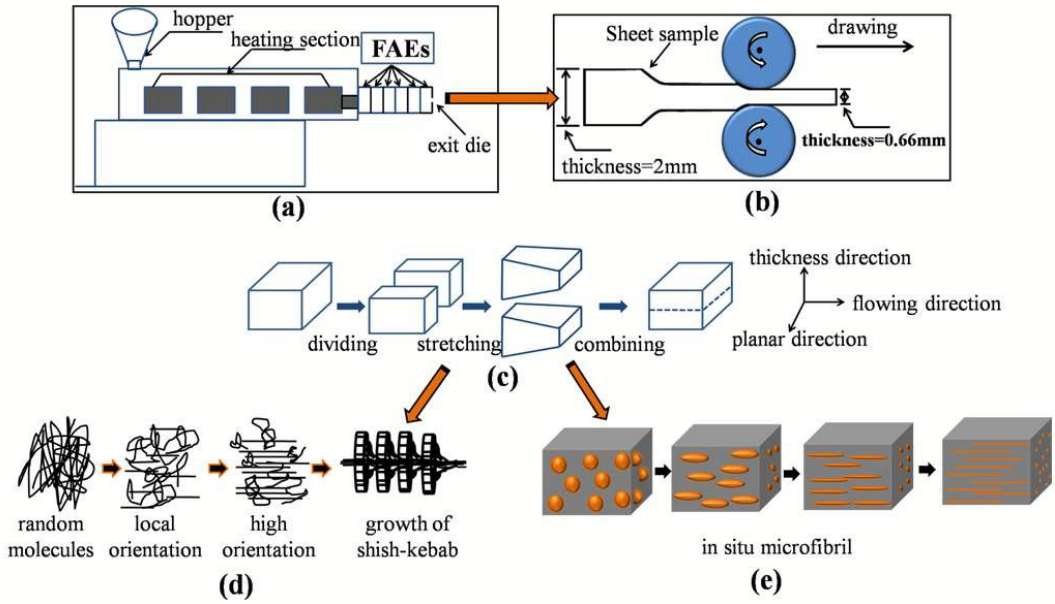

Fig.1. Schematic of the MSEDC technique. a) melted-multistage stretching extrusion part; b) subsequent drawing and calendaring part; c) melt flowing process in the force assembly element; d) the molecular evolution in the force assembly element; e) the morphological evolution of dispersed phase in the force assembly element.

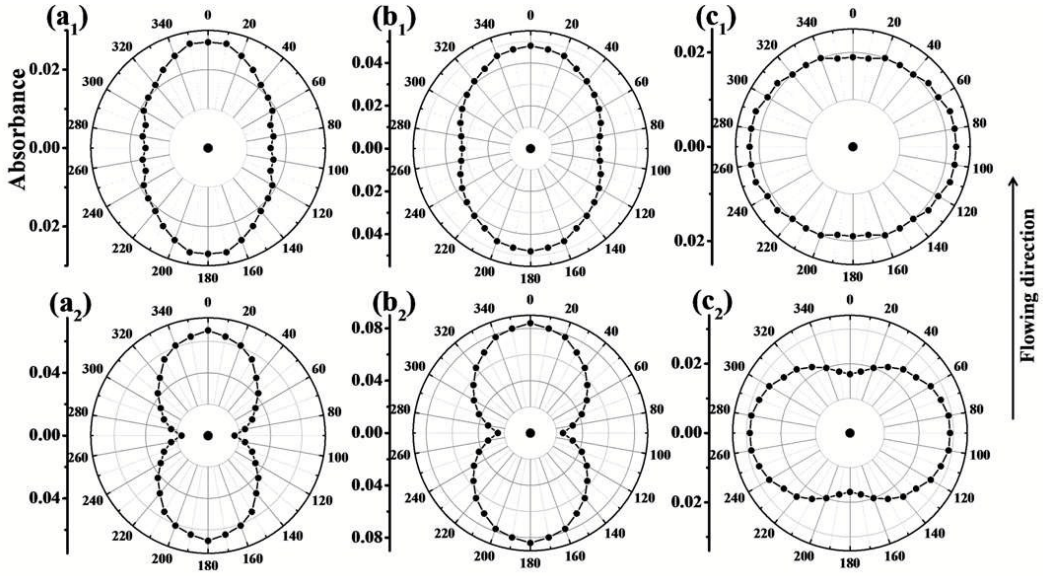

Fig.2. Polar diagrams of absorbance peaks at different positions of PP/POE blends measured by linearly polarized IR spectroscopy as a function of the angle of rotation of the film: (a), (b) and (c) are vibrations at 998cm^{-1}; 973cm^{-1} and 720 cm^{-1}, respectively. Subscript "1" and "2" represent C-20 and M-6, respectively.

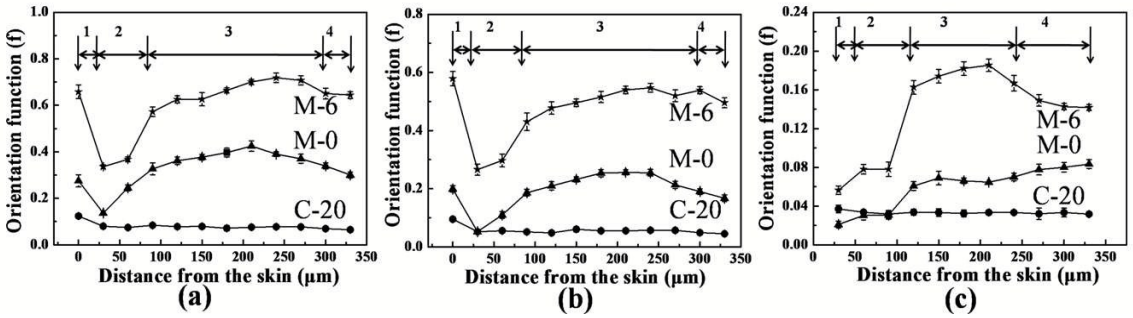

Fig.3. Distribution of orientation functions of crystalline region A) amorphous region of PP matrix, B) and hexyl side chain in POE molecular chain, C) in C-20, M-0 and M-6. 1, 2, 3, 4 in these figures represent skin layer, sub-skin layer, intermediate layer and core layer, respectively.

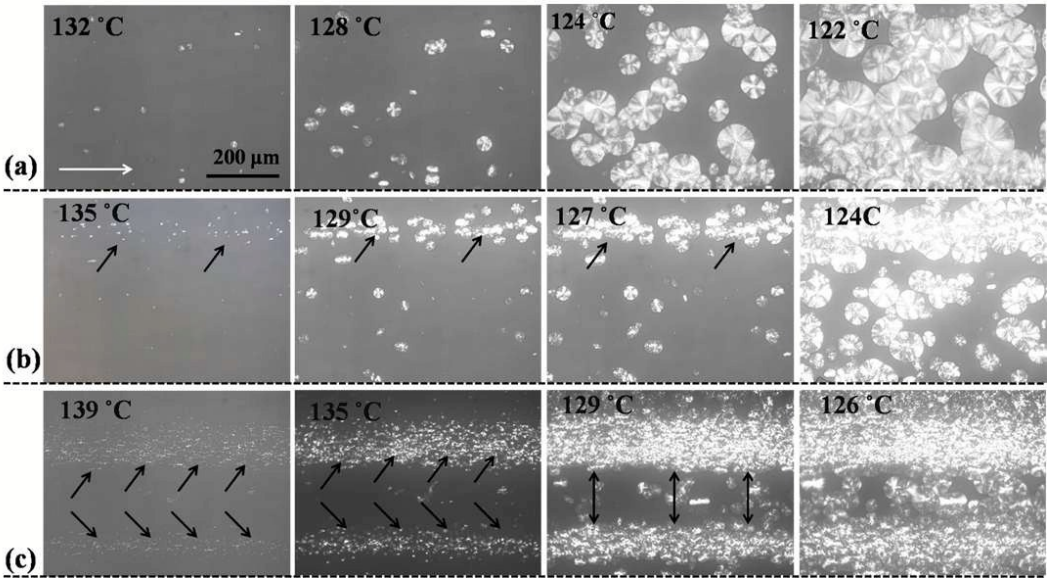

Fig.4. Optical non-isothermal cooling images of C-20 (a), M-0 (b) and M-6 (c). The white arrow indicates the melt flowing direction.

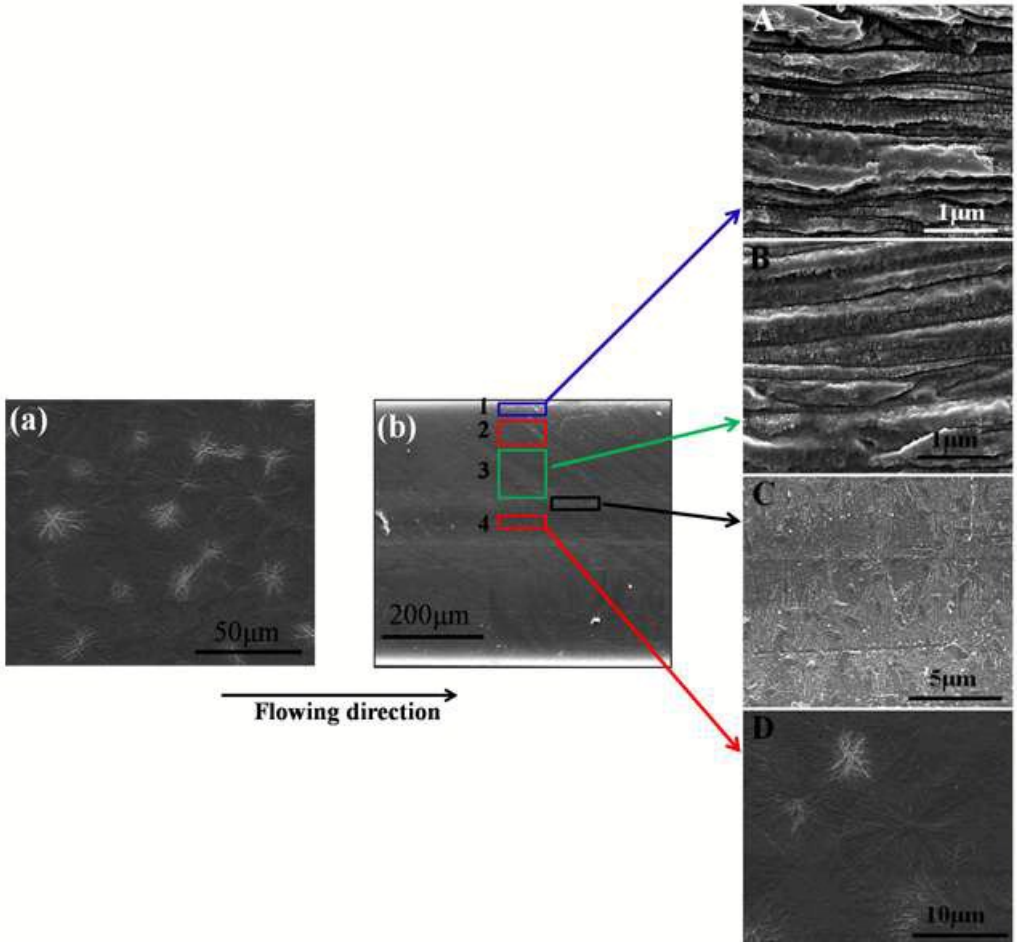

Fig.5. SEM micrographs for the crystalline structures of etched C-20 (a) and M-6 (b). 1, 2, 3, 4 in M-6 represent skin layer, sub-skin layer, intermediate layer and core layer, respectively.

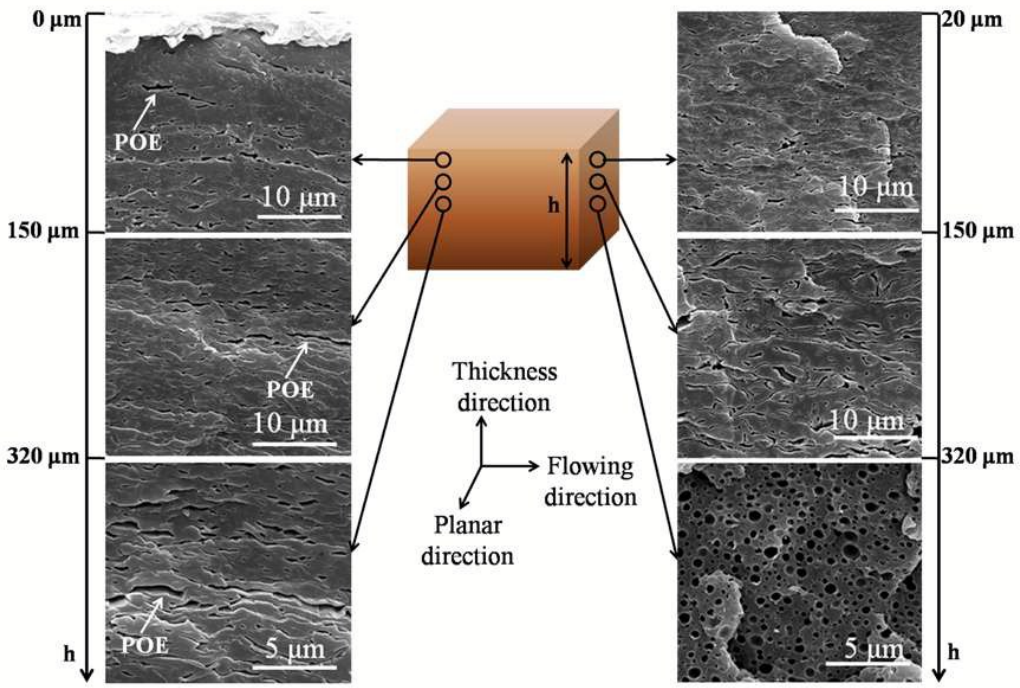

Fig.6. SEM images of heptanes etched surfaces of M-0 along the thickness direction.

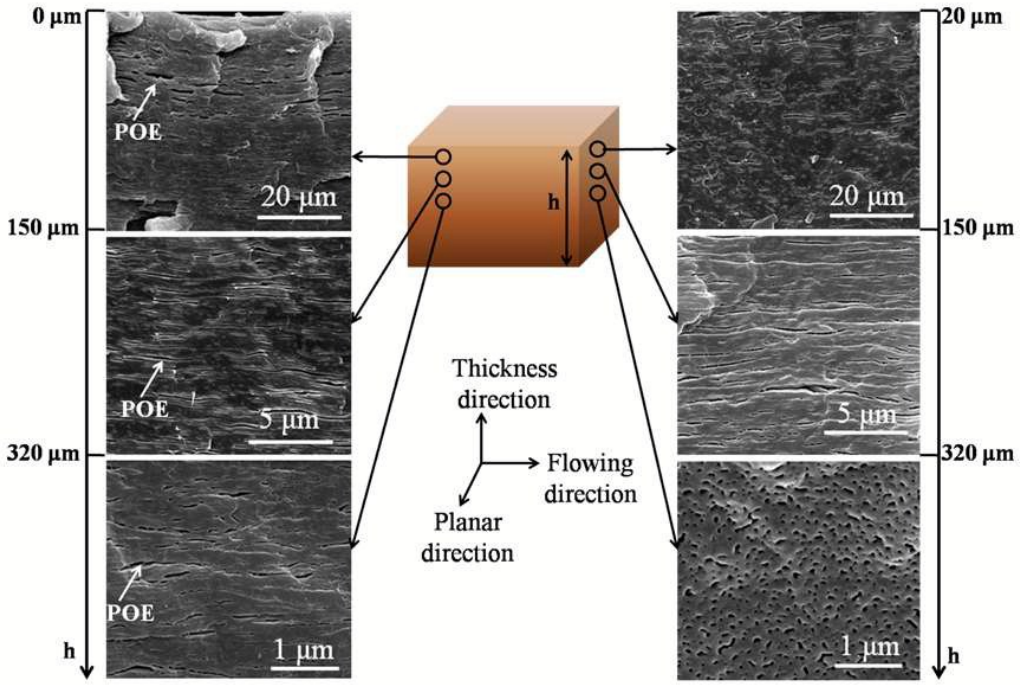

Fig.7. SEM images of heptanes etched surfaces of M-6 along the thickness direction.

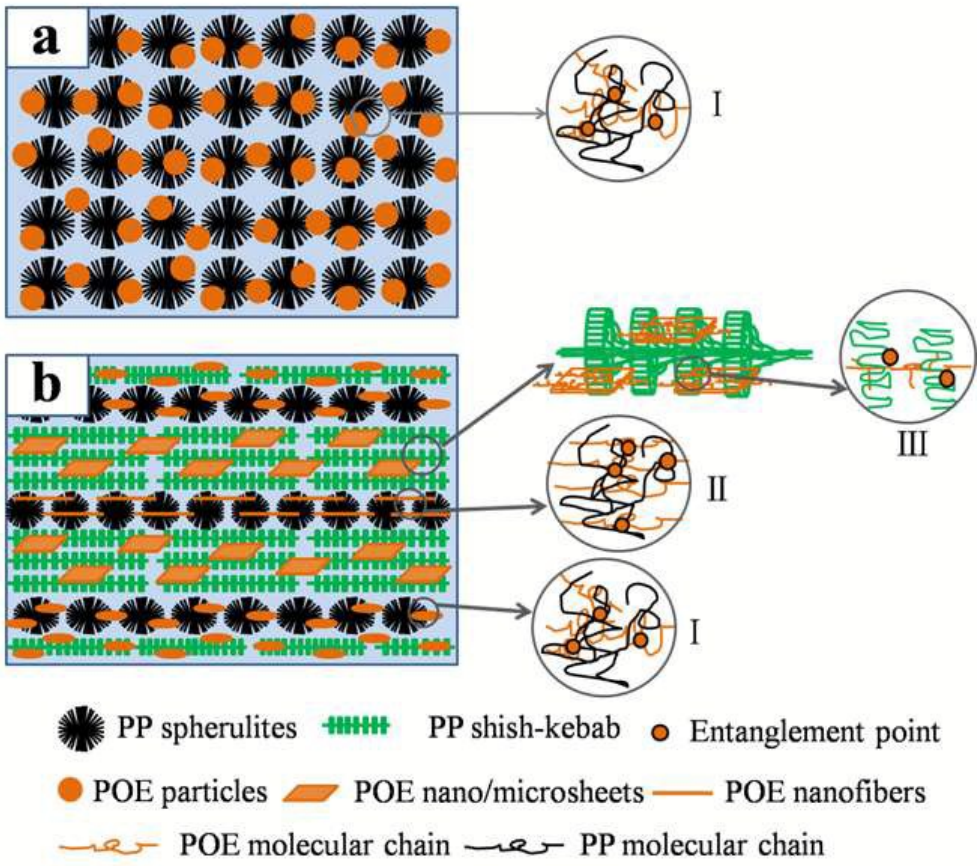

Fig.8. Schematic illustration of crystalline structure, dispersed phase morphology and molecular entanglement in C-20 (a) and M-6 (b), respectively. Note that the size of elastomer domains, the size of spherulites and shish-kebabs are not to scale.

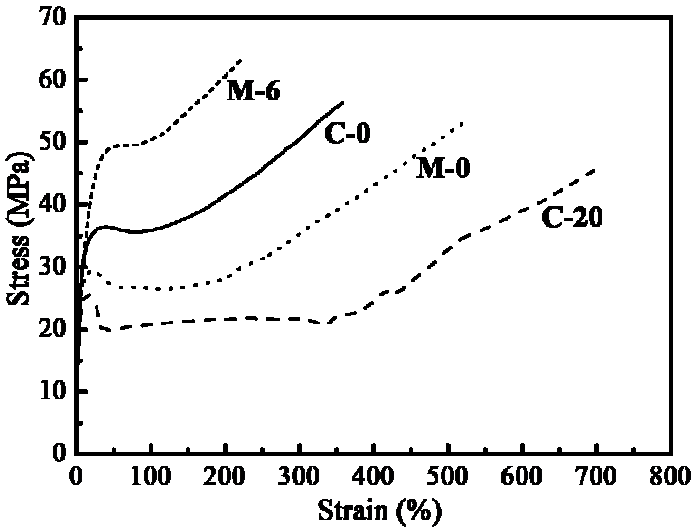

Fig.9. Typical strain-stress curves for C-0, C-20, M-0 and M-6.

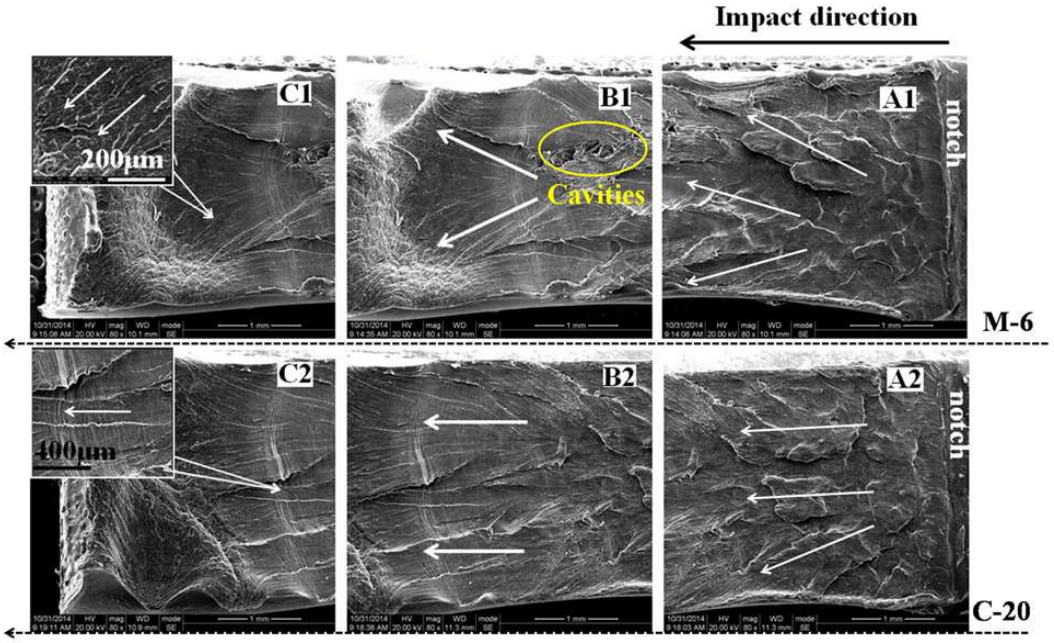

Fig.10. SEM images of impact fracture surface of M-0, and C-20. A, B, C was different regions of impacted sample with the distance away from the notch increased. The white arrows indicate the crack direction.

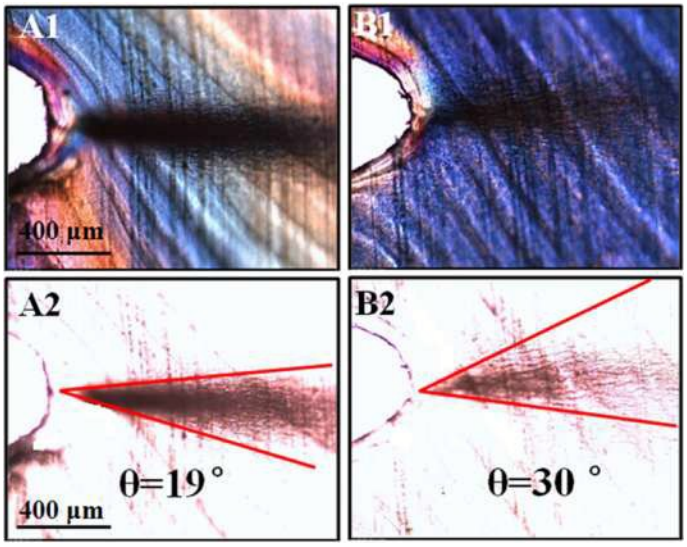

Fig.11. Propagation patterns of craze before the formation of crack in C-20 (A) and M-6 (B) after the part-impact test.

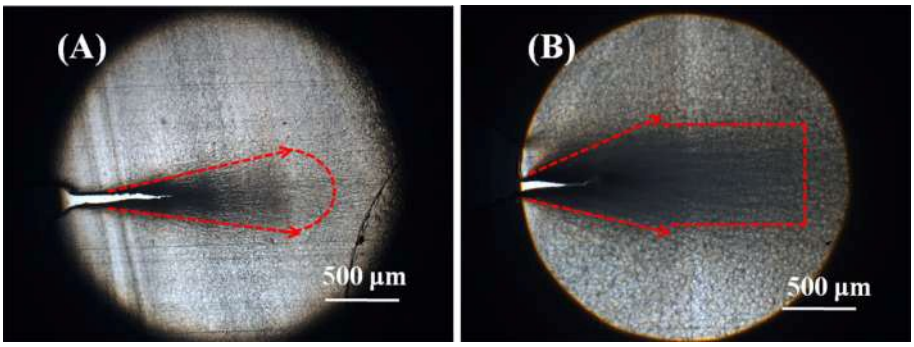

Fig.12. Propagation patterns of craze after the formation of crack in C-20 (A) and M-6 (B) after the part-impact test.

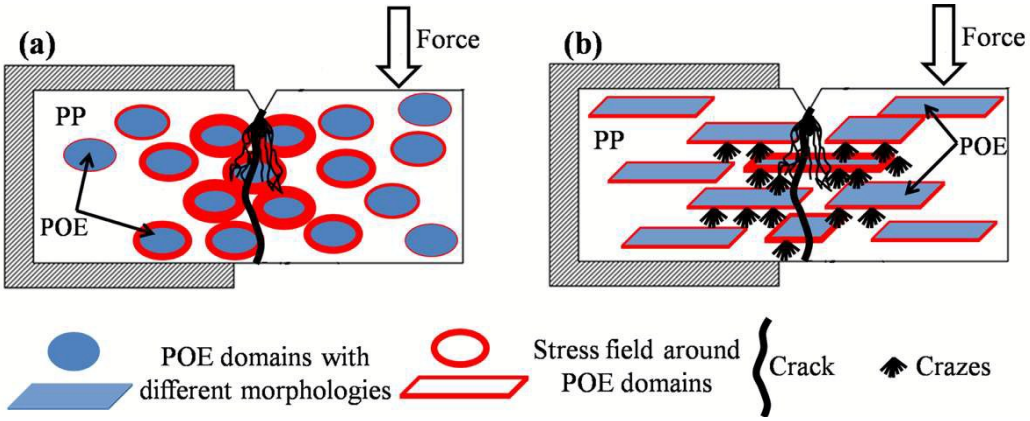

Fig.13. Sketch of impact failure mechanism of conventional PP/POE blends (a) and MSEDC blends (b).

Table of Content

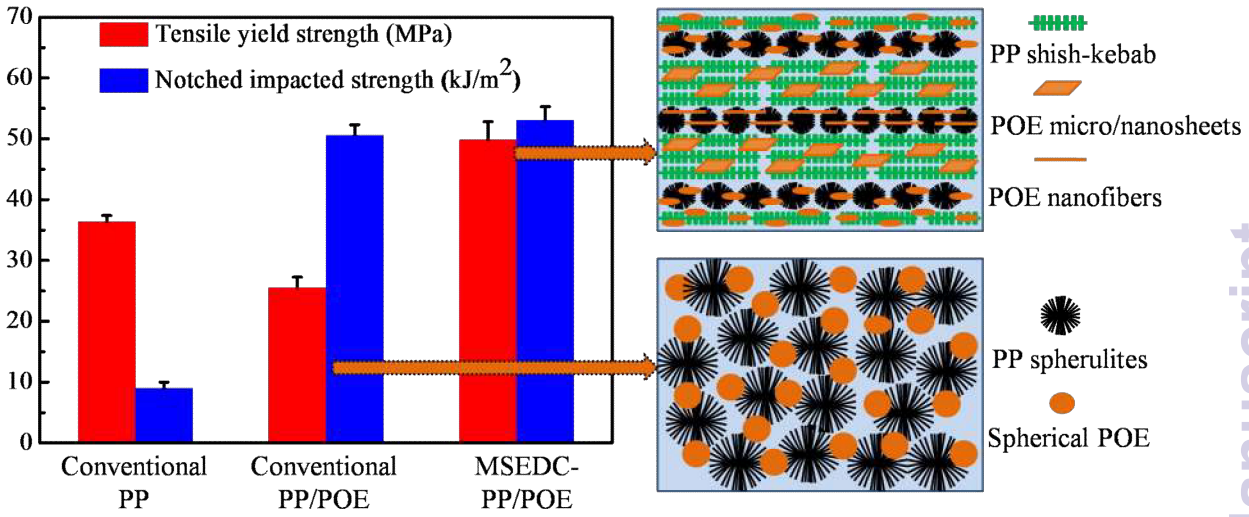

Realizing simultaneous reinforcement and toughening in polypropylene based on polypropylene/elastomer via controlling crystalline structure and dispersed phase morphology